Applied Radiation and Isotopes 161 (2020) 109141

Contents lists available at ScienceDirect

Applied Radiation and Isotopes

journal homepage: http://www.elsevier.com/locate/apradiso

Shielding effectiveness: A weighted figure of merit for space radiation shielding

J.M. DeWitt [a,*], E.R. Benton [b]

[a] Department of Physics, East Carolina University, Greenville, NC, 27834, USA
[b] Department of Physics, Oklahoma State University, Stillwater, OK, 74078, USA

A B S T R A C T

The risk to space crew health and safety posed by exposure to space radiation is regarded as a significant obstacle to future human exploration missions to the Moon, Mars, and beyond. Engineers developing future spacecraft or planetary surface habitats can benefit from detailed knowledge of a broad range of possible materials that could provide improved protection to space crews from the deleterious effects of prolonged exposure to the space radiation environment. As one step towards providing this knowledge base, we have developed an empirical weighted figure of merit, referred to as shielding effectiveness, that quantifies the ability of a candidate material to shield space crews from the space radiation environment. The shielding effectiveness, as formulated in this study, accounts for the competing physical aspects of target and projectile fragmentation to provide a comprehensive assessment of radiation protection with regard to passive shielding for space applications. The empirical data used in determining shielding effectiveness was obtained from proton and heavy ion accelerator-based experiments wherein Al_2O_3:C optically stimulated luminescence dosimeter and CR-39 plastic nuclear track detector were irradiated behind candidate space radiation shielding materials of varying composition and depth. As a test case, the experimental setup was exposed to nominal beams of 1 GeV protons, and 1 GeV/n ^{28}Si and ^{56}Fe heavy ions, the latter serving as a sample of the high linear energy transfer portion of the galactic cosmic ray spectrum. Established radiation dosimetry techniques were used to obtain linear energy transfer spectra, absorbed dose, and dose equivalent as a function of depth. Based on the measurement results, a shielding effectiveness value was computed, quantifying the efficacy of the candidate material as a function of depth, with cumulative weighting factors accounting for the measured percent composition of baryonic matter in the galactic cosmic ray spectrum, and the measured percent contribution to absorbed dose and dose equivalent. The methodology for shielding effectiveness was tested using the common materials of aluminum, copper, graphite, and water, with polyethylene serving as the standard reference. The preliminary shielding effectiveness values for these materials confirm the low Z principle for effective space radiation shielding, and, furthermore, these values tend to be lower when the effectiveness calculation is based on dose equivalent. Of the common materials studied here, at a bulkhead depth of 5 g/cm^2, all materials provide a similar level of radiation protection to within standard error. In addition, this method can be used to supplement and/or verify similar findings obtained from transport models.

1. Introduction

In preparation for long-term missions to the Moon, Mars, and beyond, designs for future human exploration missions will likely need to take into account prolonged exposure of space crews to the biologically-hazardous space radiation environment (Benton and Benton, 2001). Strategies to minimize space crew exposure to radiation will almost certainly include shield design and optimization. The implementation of radiation protection countermeasures through the addition of shielding mass has traditionally been a low priority on missions to low Earth orbit (LEO). For example, polyethylene shielding for radiation protection purposes was added to a portion of the ISS, but only after the station was already in orbit (Shavers at al., 2004). Given the exposure estimates for a human mission to Mars (Simonsen et al., 2000; Wilson et al., 1997; Wilson et al., 1999; Cucinotta and Durante, 2006; Durante, 2014), shielding may likely need to be taken into account at the outset of the design process.

The risk associated with exposure to the space radiation environment includes both deterministic and stochastic effects. The type (deterministic or stochastic) and severity of the effect is determined by which component of the space radiation environment an individual is exposed to and for how long. Deterministic endpoints are short-term biological consequences of ionizing radiation exposure that possess a threshold, such as acute radiation sickness (ARS) or the induction of cataracts in the eyes. By contrast, stochastic endpoints such as cancer are biological consequences of ionizing radiation exposure that are largely random.

The short-term exposure of an inadequately shielded individual to a solar particle event (SPE) is associated with deterministic effects that include skin burn, ARS, and cataracts with very high absorbed doses. An astronaut exposed to a major SPE can receive an absorbed dose

* Corresponding author.
E-mail address: dewittjo@ecu.edu (J.M. DeWitt).

https://doi.org/10.1016/j.apradiso.2020.109141
Received 1 July 2019; Received in revised form 11 March 2020; Accepted 19 March 2020
Available online 30 March 2020

approximately 100 times greater than that attributed to the galactic cosmic ray (GCR) spectrum (Sihver, 2008), leading to death or at least ARS. However, given the small likelihood of a major SPE (Riley, 2012), the short-term effects of inadequate shielding are of lesser concern than long-term effects.

The long-term exposure of an inadequately shielded individual to the constant, low flux of GCRs is associated with stochastic effects. The long-term exposure of personnel to the steady flux of the GCR spectrum is more problematic for missions that have a duration of 3 months or more, such as an extended mission to the Moon or a mission to Mars (Adams et al., 2007), where the development of cancer is of special concern (Cucinotta et al., 2012; Cucinotta, 2014; Cucinotta and Cacao, 2017). In general, the uncertainty as it relates to space radiation risk is associated with poor knowledge of the biological effects of exposure to GCRs; specifically the uncertainty of the quality factor related to organ dose equivalent (Durante and Cucinotta, 2011).

The cost of launching sufficient quantities of shielding to protect space crews from the whole of the space radiation environment is prohibitive using only standard materials. An attractive approach to this problem is the use of multifunctional materials—materials designed to fulfill more than one function (Wilson et al., 2001b). These materials have chemical and mechanical properties that enable them to function, for example, as part of the structure of a spacecraft or planetary surface habitat as well as space radiation shielding (NRC, 2008). The potential reduction in mass compared to inherent shielding translates into more affordable space exploration missions, while at the same time producing a more favorable radiation environment inside a spacecraft or planetary surface habitat (Badavi et al., 2010). In general, it should be noted that the optimization of mass through the use of multifunctional materials could include the replacement of a material with a more optimal alternative, the relocation of a material to a more logical position, or the repurposing of a readily available material in order to better meet the radiation protection needs of space crews.

Given the related problems of a hazardous space radiation environment and the large financial cost required to protect space crews using only standard materials, it would be advantageous if experimentally-obtained performance data specific to space radiation shielding efficacy were made available to the aerospace engineering community as a means of matching the desired mechanical characteristics of a given component with the As Low As Reasonably Achievable (ALARA) principle. Because of this, engineers and designers of future spacecraft or planetary surface habitats require a method that empirically quantifies the space radiation shielding performance of candidate materials suitable for the design and development of such structures (Wilson et al., 2001a). The goal of the present work is to address this requirement by providing an empirical method that can characterize the radiation shielding properties of candidate materials applicable to space exploration missions (DeWitt et al., 2009).

To assess the efficacy of a given space radiation shielding material, ideally one would like to expose samples of the material at varying thicknesses in situ and measure the change in the primary radiation field as a function of shielding depth. Alternatively, one could simulate such space-based experiments using either deterministic or Monte Carlo radiation transport codes; examples of such codes would be HZETRN (Wilson et al., 1995; Wilson et al., 2015; Slaba et al., 2015) and FLUKA (Ferrari et al., 2005; Böhlen et al., 2014) for deterministic and Monte Carlo, respectively. Finally, one could conduct ground-based accelerator experiments in a more controlled setting than in a space environment, as is done in this study. A major shortcoming of the ground-based accelerator experiment approach is that one is usually restricted to using mono-energetic heavy ion beams of fixed Z. While the results of such experiments would be valid for that particular ion, they say little about the remaining particle species that make up the GCR spectrum.

An improvement on the ground-based accelerator approach would be to use a variety of different ions of Z and E that are representative of the GCR spectrum (Norbury et al., 2016). A challenge associated with this approach lies in the proper assessment of the results of such experiments and their relationship to the actual GCR charge and energy spectrum. The goal of this work is to address this challenge by presenting an empirically-based weighted figure of merit approach. In contrast to a model-based figure of merit (Wilson et al., 1993), the shielding effectiveness presented here is weighted according to the percent fraction of baryonic components of the GCR spectrum (Simpson, 1983), in addition to the measured contributions to absorbed dose and dose equivalent accrued by an individual in transit to Mars (Zeitlin et al., 2013; Zeitlin, 2016), also represented in terms of percent fraction.

The intent of the described method is to provide experimental knowledge of space radiation shielding efficacy as encapsulated in the definition of shielding effectiveness (Section 2). While it is true that experimentally the method can only sample a limited fraction of the GCR spectrum, a major advantage is the ability of the method to empirically account for the material composition of each shielding candidate, especially in the case of novel and/or complex materials. In this way an empirically-based figure of merit—in the form of shielding effectiveness—acts to supplement and/or verify those produced by transport models. Moreover, the methodology described here can accommodate additional data from previously unavailable ion beams as they become active in the future.

The empirical method presented here uses dosimetric data that is measured behind a variety of shielding targets at multiple depths to formulate the shielding effectiveness relative to polyethylene, which serves as the informal space radiation shielding standard (Guetersloh et al., 2006). The shielding effectiveness is based on the dosimetric quantities of absorbed dose and dose equivalent, and is weighted to account for the complexities of the space radiation environment that will be encountered by space crews. Our suggested method synthesizes the results of many space radiation shielding measurements made using CR-39 PNTDs that were exposed to a number of experimentally available proton and heavy ion beams at the NASA Space Radiation Laboratory at the Brookhaven National Laboratory (BNL NSRL). These results are used to compute the shielding effectiveness as a function of shielding depth in order to quantify the efficacy of a candidate space radiation shielding material.

2. Shielding effectiveness

The shielding effectiveness S is defined as the weighted sum of the proton + alpha particle contributions S_p plus the heavy ion (HI) contribution S_{HI}:

$$S = aS_p + bS_{HI}, \tag{1}$$

The coefficients a and b that weight the S_p and S_{HI} terms in Equation (1) arise as averages of two competing phenomena: One is the fact that protons + alphas constitute approximately 99% of the baryonic portion of the GCR spectrum, with the remaining 1% composed of heavy ions (Simpson, 1983). The other is the observation that protons + alphas contribute approximately 70% of the measured absorbed dose to an individual traveling outside the Earth's atmosphere and magnetosphere, with heavy ions contributing the remaining 30% (Zeitlin et al., 2013; Zeitlin, 2016). With regard to absorbed dose, the coefficients of shielding effectiveness are $a = (0.99 + 0.70)/2 = 0.845$ and $b = (0.01 + 0.30)/2 = 0.155$. With regard to dose equivalent, however, these coefficients change to $a = (0.99 + 0.20)/2 = 0.595$ and $b = (0.01 + 0.80)/2 = 0.405$ since heavy ions contribute approximately 80% of the measured dose equivalent (Zeitlin, 2016). In general, the coefficient a tends to encapsulate a degradation in shielding performance (absorbed dose increase), while the coefficient b translates into an enhancement of the same (absorbed dose decrease). This weighting strategy via averages provides an intuitive way of capturing the "quality versus quantity" phenomenon inherit in GCR passage through space radiation shielding. Specifically, the coefficient a recognizes the fact that while the quantity

of GCR protons dominates the absorbed dose contribution in the shielding metric, the dose equivalent impact, by contrast, is diminished due to their relatively small LET-dependent quality factor. Conversely, the coefficient b recognizes the fact that while the quantity of GCR heavy ions comprise only a relatively small percent fraction of the GCR spectrum, they nonetheless contribute substantially to dose equivalent due to their high LET-dependent quality factor.

Since alpha particle irradiations were not performed in this study, the factor S_p is the normalized absorbed dose reduction due to protons only:

$$S_p(x) = \frac{D_{PE}(x)D_{abs}(0)}{D_{PE}(0)D_{abs}(x)}, \tag{2}$$

where the factors $D_{PE}(0)$ and $D_{abs}(0)$ are the absorbed dose values measured from CR-39 PNTD at the front of target-detector stacks composed of polyethylene (PE) and an absorber of interest (abs), respectively. In similar fashion, the factors $D_{PE}(x)$ and $D_{abs}(x)$ are the absorbed dose values measured from CR-39 PNTD at a depth x within target-detector stacks composed of polyethylene and an absorber of interest, respectively. It should be noted that Equation (2) does not exclude the possibility of a shielding effectiveness greater than 1 due to a combination of ion kinetic energy, absorber type, and absorber thickness. The factor S_{HI} is the normalized absorbed dose reduction due to heavy ions:

$$S_{HI}(x) = \frac{\sum_i [Z^2 D_{PE}(x)/D_{PE}(0)]_i}{\sum_i [Z^2 D_{abs}(x)/D_{abs}(0)]_i}, \tag{3}$$

where the numerator and denominator are the sums over experimentally available GCR species Z and their associated absorbed dose measurements; the remaining factors hold the same meaning as in Equation (2). The square of the atomic number accounts for the fact that LET and therefore absorbed dose is proportional to Z^2. The normalization technique adopted here ensures that the contribution from heavy ions is not given undue weight to the shielding effectiveness. Using these empirical quantities, Equation (1) is rewritten, giving shielding effectiveness as a function of depth $S(x)$:

$$S(x) = a\frac{D_{PE}(x)D_{abs}(0)}{D_{PE}(0)D_{abs}(x)} + b\frac{\sum_i [Z^2 D_{PE}(x)/D_{PE}(0)]_i}{\sum_i [Z^2 D_{abs}(x)/D_{abs}(0)]_i}, \tag{4}$$

For polyethylene, $a(1) + b(1) = 1$ as a baseline value. The scaling methodology adopted in Equation (4) attempts to address the observation that, experimentally, the method can only sample a limited fraction of the GCR spectrum. The shielding effectiveness metric $S(x)$ represents the ability of a given material to adequately shield space crews from the effects of a harmful space radiation environment.

3. Materials and methods

Dosimetric data behind varying depths of common materials were measured using CR-39 PNTD—a tissue-equivalent passive radiation detector—when exposed to nominal beams of 1 GeV protons, and 1 GeV/n ^{28}Si and ^{56}Fe heavy ions available at the NASA Space Radiation Laboratory at the Brookhaven National Laboratory (Brown et al., 2010). CR-39 is a transparent cross-linked thermoset polymer having the molecular formula $C_{12}H_{18}O_7$. This type of polymer has been used as a radiation detector since 1978 and remains the most sensitive, as well as the most commonly used, solid state nuclear track detector (SSNTD) in use today. CR-39 PNTD was first used as a SSNTD by P.B. Price (Cartwright et al., 1978) for cosmic ray research and by E.V. Benton (Cassou and Benton, 1978) for radiation dosimetry. The detector is sensitive to charged particles of LET-in-water between 5 and 1500 keV/μm, which includes protons of kinetic energy less than 10 MeV, α-particles of kinetic energy less than 200 MeV, and heavy ions with atomic number greater than 3 of all kinetic energies. Neutrons of energy between 1 and 20 MeV can be detected via tracks from recoil protons produced in neutron interactions with the hydrogen nuclei in the PNTD. Higher energy protons and neutrons can be detected via inelastic target fragmentation reactions with the carbon and oxygen nuclei of the PNTD, or in target materials immediately adjacent to the detector. It should be noted that dosimetric data corresponding to neutron contributions was not included in our processing of the passive detectors. The use of CR-39 PNTD is part of an established radiation dosimetry technique that was used to measure normalized differential linear energy transfer (LET) fluence spectra, absorbed dose, and dose equivalent as a function of shielding depth (Zhou, 2012).

Absorbed dose due to protons was measured with aluminum oxide, an optically stimulated luminescence dosimeter (OSLD), which is an insulating crystalline substance doped with carbon having the molecular formula Al_2O_3:C. Al_2O_3:C is sensitive to charged particles of all LET, but to charged particles of LET greater than 5 keV/μm with reduced efficiency. The relative luminescence efficiency of the Al_2O_3:C dosimeters used in this study varies with LET; for the case of 1 GeV nominal energy protons (approx. 0.2 keV/μm), the relative efficiency is 1.00 ± 0.05, indicating that the ability of the dosimeter to measure absorbed dose is unaffected (Sawakuchi et al., 2008). Furthermore, for the variety of low- and high Z target materials used in this study, the proton beam transfers approximately 10 MeV of kinetic energy (resulting in a negligible change in the LET) to the absorber over a depth of 20 g/cm^2, suggesting an unaffected detector efficiency even at relatively large shielding depths (Weaver and Westphal, 2002).

The intensity of the emitted light during stimulation is proportional to the absorbed dose accrued during the original exposure of the crystal to ionizing radiation. In this work, the Al_2O_3:C OSLDs were stimulated with a green LED and the intensity of the luminescence signal was monitored in the UV range (ultraviolet, UV: U-340 filter, 300–380 nm). The Al_2O_3:C OSLDs were read-out using a Risø TL/OSL DA-15 reader (Rink and Thompson, 2013). In contrast to CR-39 PNTD, it should be noted that the OSL detectors used in this study do not provide a differential LET fluence spectrum, but instead only yield individual absorbed dose values. Absorbed dose from OSL was obtained based on individual OSLD calibrations with a standard ^{90}Sr beta particle source. As with CR-39 PNTD, the use of Al_2O_3:C is also part of an established radiation dosimetry technique that was used to measure absorbed dose only (McKeever, 2011).

3.1. Experimental setup

The dosimetric quantities used for the calculation of the shielding effectiveness were LET fluence spectrum, absorbed dose, and dose equivalent. As a test case, these quantities were measured behind targets of common materials as a function of shielding depth for mono-energetic proton and heavy ion beams. Measurements were made using stacks of CR-39 PNTD and Al_2O_3:C OSLD in front of- and behind the target material. The shielding targets were exposed to proton, ^{28}Si, and ^{56}Fe beams with actual kinetic energies of 996 MeV, 975 MeV/n, and 956 MeV/n, respectively. The actual kinetic energies of the beams at the front of the shielding targets were determined by measuring Bragg curves at the accelerator and determining the ranges of the beams in water. The 1 GeV nominal kinetic energy of the proton beam corresponds to an LET-in-water value of 0.22 keV/μm (range in water: 328.7 cm); the 1 GeV/n nominal kinetic energy of the heavy ion beams corresponds to LET-in-water values of 44.1 and 153.9 keV/μm (ranges in water: 44.4 cm and 24.9 cm) for the ^{28}Si and ^{56}Fe beams, respectively (Weaver and Westphal, 2002). Each irradiation was conducted with a fluence of approximately 5,000 ions per cm^2 to minimize the number of overlapping tracks in the CR-39 PNTD. The detectors were exposed with the standard wide field geometry that specifies a beam size of at least 10×10 cm and a minimum beam uniformity of 90%. Fluence was monitored and the beam was stopped by means of a fast cut-off plastic scintillator system.

The CR-39 PNTDs ($4.0 \times 4.0 \times 0.06$ cm) placed at each depth of shielding material in the experimental setup were arranged in groups of four to form a sub-stack (see Figs. 1 and 2). A similar configuration was adopted for the proton irradiations, where CR-39 PNTD was replaced by Al_2O_3:C OSLD. As shown in Fig. 1, the experimental setup for all irradiations consisted of arranging CR-39 PNTD sub-stacks and layers of shielding material to form a detector-target stack. The CR-39 PNTD sub-stacks were arranged in a staggered configuration so that the beam propagated through the intended depth of shielding material for each sub-stack. The front CR-39 PNTD sub-stack (no target, 0 g/cm^2) sampled the mono-energetic beam before it propagated through the detector-target stack and served to verify the properties of the incoming beam. Successive CR-39 PNTD sub-stacks sampled the beam at successive shielding depths in order to determine how the shielding material modified the radiation field as a function of depth. The detector-target stack was exposed normal (i.e., 90°) relative to the direction of the incident beam. In this way, a differential LET fluence spectrum, normalized to the fluence measured in the front CR-39 PNTD, was measured from the primary beam as well as from secondary projectile fragments.

Following irradiation, two of the four CR-39 PNTDs from each CR-39 PNTD sub-stack were chemically etched in 6.25 N NaOH solution at 50 °C for 168 h (7 days) and 36 h, yielding bulk etch values of approximately 40 and 8 μμm, respectively. The bulk etch was determined using the Henke-Benton method (Henke et al., 1986). The Al_2O_3:C OSLDs required no post-exposure processing, and only needed to be read-out using the Risø TL/OSL DA-15 reader. A Samaica nuclear track detector analysis system manufactured by ELBEK GmbH, Siegen, Germany was used to carry out semi-automatic measurement and analysis of each exposed CR-39 PNTD analyzed for this work (Dreute et al., 1986; Noll et al., 1988; Rusch et al., 1991; Trakowski et al., 1984; Wiegel et al., 1986). A total of about 15,000 tracks within an area of roughly 3 cm^2 were typically measured. The track detector analysis system returns essential track information including the semi-major and semi-minor axes, the sine of the angle of the major axis of a track with respect to the x-axis, and the central brightness gray scale value of a track.

Following analysis of a CR-39 PNTD surface by the ELBEK system, the list of accepted track data was processed using a custom-written Fortran program that generated a differential LET fluence spectrum—normalized to the incident particle fluence—through the following steps: 1) the reduced etch rate ratio of each track was determined based on its measured semi-major and -minor axes, and normalized by the bulk etch; 2) the LET_{200}CR-39 of each track was calculated using the empirically measured detector response function shown in Fig. 3; 3) the LET_{200}CR-39 value of each track was converted to $LET_{\infty}H_2O$ (Benton et al., 2010); 4) the $LET_{\infty}H_2O$ values of all valid tracks were sorted into bins of 1 keV/μm width, each of which were divided by the size of the scanned area and the incident primary projectile fluence as measured in the front (no target, 0 g/cm^2) CR-39 PNTD, resulting in a normalized differential LET fluence spectrum, an example of which is shown in Fig. 4. A spectrum such as this can be integrated to obtain absorbed dose and dose equivalent from charged particles only.

3.2. Selection of shielding materials and depths

The space radiation environment and its interaction with matter (biological and inanimate) is an extensive subject. As such, some general statements regarding the focus of this work—which influenced the selection criteria of the candidate materials—can be listed as follows:

1. Because human health and safety are of primary concern, shielding designs need to be conservative and adhere to the ALARA principle.
2. The materials out of which spacecraft or planetary surface habitats are fabricated must be lightweight and possess desirable structural, mechanical, and thermal characteristics in addition to their space radiation shielding properties.
3. It would be advantageous if experimentally obtained performance data specific to space radiation shielding efficacy were made available to the aerospace engineering community as a means of matching the desired mechanical and physical characteristics of a given component or system with the ALARA principle.
4. Given our current understanding of radiation physics, it is unlikely that any material will be developed in the near future that will yield spectacular improvements in space radiation shielding effectiveness.
5. The materials relevant for use in aerospace design may have consequences that are desirable (e.g., projectile fragmentation) or undesirable (e.g., secondary neutron production) with regard to the internal radiation environment inside a proposed spacecraft or planetary surface habitat.

Based on the observations listed above, the common materials aluminum, copper, polyethylene, graphite, and water are considered in this study because they are 1) frequently present in current spacecraft design, 2) chemically or compositionally well-defined, and/or 3) have physical properties that make them relevant points of interest with regard to the space radiation shielding experiments.

As a basic test of the shielding metric described by Equation (4), we have chosen a set of baseline target materials that include aluminum, copper, graphite, and water. Additionally, polyethylene was chosen as the standard reference in assessing space radiation shielding performance (Guetersloh et al., 2006; Thibeault et al., 1997) because it is (1) the most common organic solid with the highest hydrogen concentration by mass and is (2) an effective space radiation shielding material due to its chemical stability (non-reactivity) and low Z. Aluminum was selected because of its common use in spacecraft construction; the use of copper represents something of a worst case scenario since most spacecraft contain a non-trivial amount of copper in the form of electrical wiring and components. Water was selected because it is 1) hydrogen-rich (i.e., low Z), 2) contains an ^{16}O nucleus that is stable given its doubly "magic" number of protons and neutrons, and is 3) a critical consumable for any manned spacecraft or planetary surface habitat.

Graphite occupies a special significance in this study because 1) the molecular formula of polyethylene, $(CH_2)_n$, contains carbon and 2) this carbon component has an atomic mass that is divisible by 4. The first point forms the basis of a comparison with the polyethylene standard. The second point is significant because of the tendency of carbon to decompose into α-particles (^{4}He nuclei) rather than neutrons during nuclear interactions. The stability of α-particles is due to their relatively high binding energy; the non-zero electric charge permits their stopping in ordinary matter. Graphite was also selected because it is a component of carbon composites. Such composites are increasingly being used in the air frames of next-generation commercial airliners such as Boeing's 787 Dreamliner and Airbus's A350. The mechanical and radiation shielding properties of carbon fibers and carbon composites could possibly enable them to function as the multifunctional superstructure of future spacecraft or planetary surface habitats (NRC, 2008; Konradi and Cucinotta, 1997).

The dosimetric measurements were carried out at shielding depths relevant to the design and development of a spacecraft or planetary surface habitat: 5–20 g/cm^2 in 5 g/cm^2 intervals. The starting point of 5 g/cm^2 was chosen since this is representative of the average depth of the ISS bulkhead (Armstrong and Colborn, 2001). The end point of 20 g/cm^2 simulated a storm shelter depth (Townsend et al., 1992) as well as being representative of the average depth at the center of an ISS module (Armstrong and Colborn, 2001). By way of comparison, as much as 50 g/cm^2 may be required on interplanetary spacecraft if the recommended astronaut exposure limit is not to be exceeded, and if one were to use, for example, aluminum (Wilson et al., 2001a).

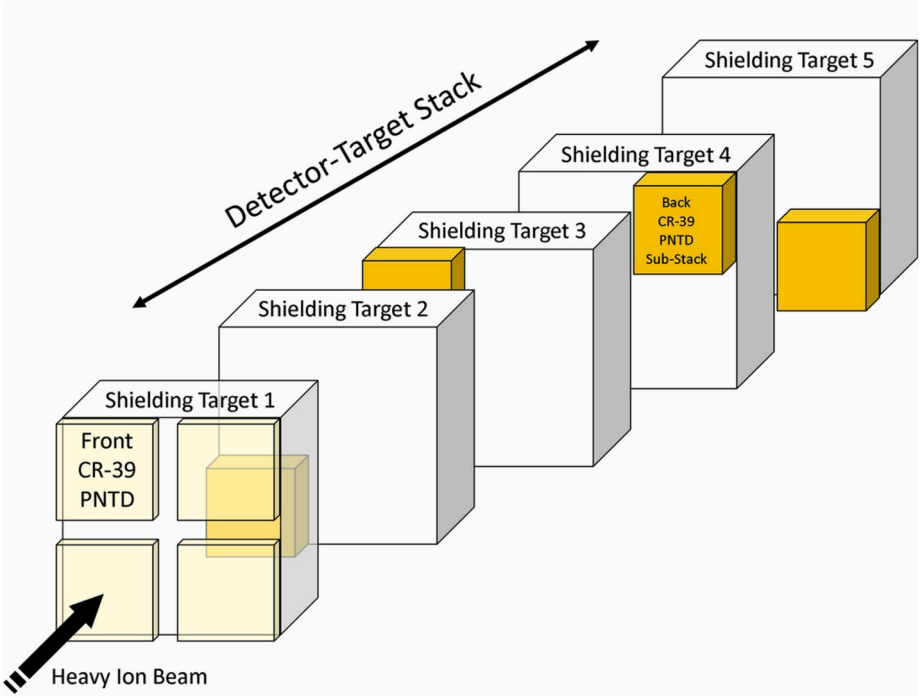

Fig. 1. The experimental setup for the heavy ion irradiations consisted of arranging CR-39 PNTD sub-stacks and layers of shielding material to form a detector-target stack. A similar configuration was adopted for the proton irradiations, where CR-39 PNTD was replaced by Al_2O_3:C OSLD.

3.3. Selection of ion beams

The GCR spectrum contains relatively significant quantities of ions of $Z = 1$, 2, 6, 8, 12, 14, and 26. A combination of these ions at 1–5 GeV/n—close to the GCR energy spectrum maximum (Badhwar, 1997)—can collectively serve as a proxy for the whole of the GCR spectrum. Unfortunately, not all of these ions are readily available in the kinetic energy range of 1–5 GeV/n from particle accelerator facilities such as the BNL NSRL and the Heavy Ion Medial Accelerator in Chiba at the National Institute of Radiological Sciences (NIRS HIMAC) in Japan. However, some groups of ions in the GCR spectrum appear in relatively significant quantities such that an ion that is readily available at an accelerator could represent the group of ions of similar Z. For example, the {^{24}Mg, ^{28}Si} group could be represented by ^{28}Si and the {^{52}Cr, ^{56}Fe} group could be represented by ^{56}Fe.

The choice of heavy ion beams used in this study was limited by 1) practical considerations such as the availability of project funds as well as accelerator time and 2) completeness of the data set. This data set was assembled from heavy ion exposures that used the baseline materials of aluminum, copper, polyethylene, graphite, and water at depths from 0 to 20 g/cm^2 in 5 g/cm^2 increments. This project performed exposures with intermediate beams such as ^{16}O and ^{20}Ne, but due to beam time constraints only a few data points were available from those experiments; their incompleteness rendered them unusable for this study. As a result the shielding effectiveness approach described here is tested using the nominal 1 GeV proton, and 1 GeV/n ^{28}Si and ^{56}Fe heavy ion exposures performed at the BNL NSRL. While this choice of heavy ion beams is by no means complete, it nonetheless contains ions at the extreme ends of the GCR spectrum (^{1}H and ^{56}Fe) as well as one intermediate beam (^{28}Si). Thus, the number obtained here can still serve as a basic test of the shielding metric. Future work could extend the proposed method by experimentally adding results from additional heavy ion beams, or by utilizing an appropriate Monte Carlo transport code, for example.

4. Results

As an illustration of the use of Equation (4), the shielding effectiveness behind 5 g/cm^2 of aluminum is computed in detail:

The proton-only contribution yields $D_{PE}(5)/D_{PE}(0) = 1.28$ and $D_{abs}(5)/D_{abs}(0) = 1.28$, which results in $S_p(5) = 0.845 \pm 0.030$ when the factor of $a = 0.845$ is used in Equation (4). The heavy ion contribution gives $\sum_i [Z^2 D_{PE}(5)/D_{PE}(0)]_i = 648$ and $\sum_i [Z^2 D_{abs}(5)/D_{abs}(0)]_i = 767$, which results in $S_{HI}(5) = 0.131 \pm 0.002$ when the factor of $b = 0.155$ is used in Equation (4). The shielding effectiveness with regard to absorbed dose D behind 5 g/cm^2 of aluminum is therefore $S_D(5) = 0.976 \pm 0.030$ to three significant figures. (For comparison, at the storm shelter depth, or 20 g/cm^2, the shielding effectiveness of aluminum is lowered to $S_D(20) = 0.865 \pm 0.027$.) By the same method, and using coefficients ($a = 0.595$, $b = 0.405$) and measured data corresponding to dose equivalent H, the shielding effectiveness values behind 5 and 20 g/cm^2 come to $S_H(5) = 0.939 \pm 0.022$ and $S_H(20) = 0.810 \pm 0.020$, respectively. (The quality factor for 1 GeV nominal energy protons is taken as 1.) The complete set of results for aluminum is presented in Table 1 to three significant figures; additional results for copper, graphite, and water are given in Tables 2–4, respectively. The shielding effectiveness for any given material at a specific depth can be compared to the reference value of 1.000 corresponding to polyethylene.

The shielding effectiveness for a variety of test materials as a function of depth in Fig. 6 was computed using Equation (4). A shielding effectiveness value S as defined in this work quantifies the ability of a given space radiation shielding material to reduce absorbed dose and dose equivalent at a given depth x. For a set of shielding effectiveness values at a particular depth, the $S(x)$ value nearest (or exceeding) 1.000 means that the corresponding space radiation shielding material performs well relative to the standard of polyethylene. The complete set of measured reference data, normalized to the front (0 g/cm^2) detector, for polyethylene is given in Fig. 5; corresponding sets for aluminum, copper, graphite, and water appear qualitatively similar. The uncertainties

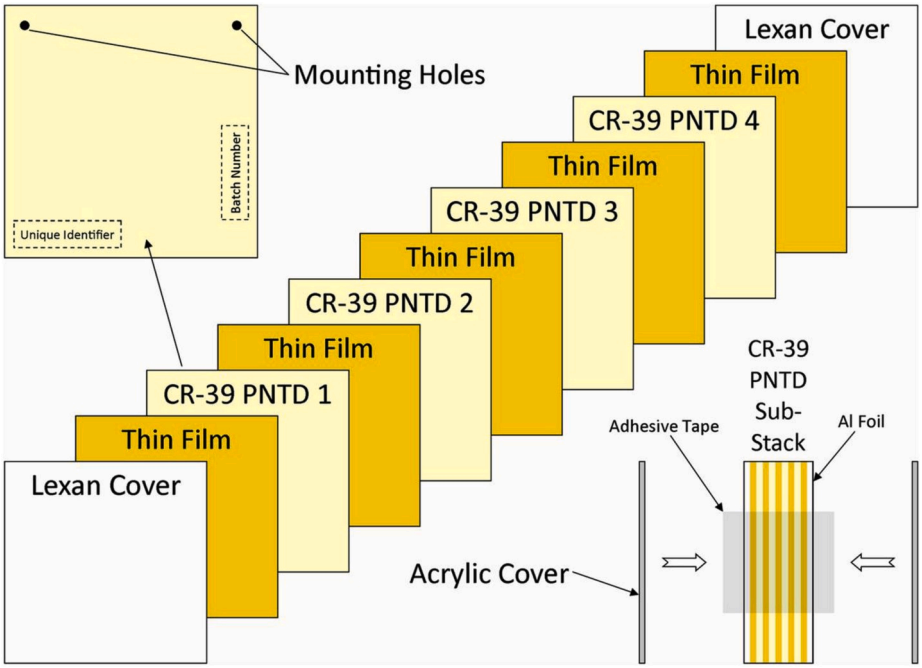

Fig. 2. Assembly of the CR-39 PNTD sub-stack. The upper left-hand corner shows placement of the mounting holes, the unique identifier, and the batch number on the CR-39 PNTD. The lower right-hand corner shows the final assembly of the CR-39 PNTD sub-stack for transport to and from the accelerator.

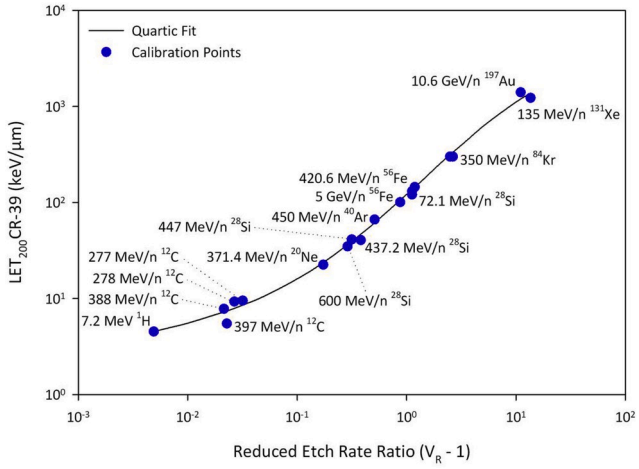

Fig. 3. Measured calibration points and the fitted response function for CR-39 PNTD (batch 29U4) when etched for 7 days (168 h).

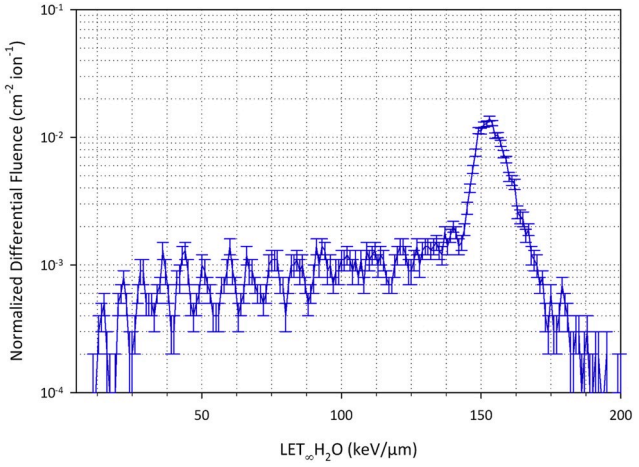

Fig. 4. The normalized differential LET fluence spectrum measured behind 5 g/cm^2 of polyethylene following exposure to a 5000 cm^{-2} 956 MeV/n^{56}Fe beam at the BNL NSRL.

shown in this figure are typical of all dosimetric data used in computing shielding performance.

Fig. 6 shows shielding effectiveness relative to polyethylene as a function of depth based on absorbed dose (A), $S_D(x)$, and dose equivalent (B), $S_H(x)$, of aluminum, copper, graphite, and water. The figure illustrates the principle of effective space radiation shielding by showing that low Z materials are generally more effective than higher Z materials in reducing absorbed dose and dose equivalent at depths greater than 5 g/cm^2. This seems to indicate that Equation (4) is formulated in a manner that is compatible with other shielding studies.

On a depth-by-depth basis, Fig. 6B, based on dose equivalent, displays shielding effectiveness that is generally lower than Fig. 6A, based on absorbed dose. This is due to the greater (measured) weight given to the heavy ion contribution in $S_H(x)$, where projectile fragmentation dominates the shape of the dose-depth profile, resulting in reduced dose equivalent. This is most pronounced in S_H(15 g/cm^2), where a significant minimum is observed in graphite, aluminum, and copper. In general, water performs quantitatively the best relative to polyethylene, while copper performs the worst, a finding that is compatible with current space radiation shielding principles. Examining performance at specific depths, aluminum, copper, and graphite are most effective at 5 g/cm^2 (typical spacecraft bulkhead thickness). Depths larger than 5 g/cm^2 tend to make the resulting radiation field more hazardous compared

Table 1
Shielding effectiveness relative to polyethylene at discrete depths of **aluminum** based on absorbed dose and dose equivalent.

Depth (g/cm^2)	S_D	S_H
5	0.976 ± 0.030	0.939 ± 0.022
10	0.886 ± 0.024	0.858 ± 0.018
15	0.871 ± 0.029	0.811 ± 0.021
20	0.865 ± 0.027	0.810 ± 0.020

Table 2
Shielding effectiveness relative to polyethylene at discrete depths of **copper** based on absorbed dose and dose equivalent.

Depth (g/cm^2)	S_D	S_H
5	0.977 ± 0.034	0.926 ± 0.025
10	0.887 ± 0.031	0.833 ± 0.022
15	0.843 ± 0.032	0.761 ± 0.023
20	0.816 ± 0.025	0.739 ± 0.018

Table 3
Shielding effectiveness relative to polyethylene at discrete depths of **graphite** based on absorbed dose and dose equivalent.

Depth (g/cm^2)	S_D	S_H
5	0.994 ± 0.056	0.983 ± 0.040
10	0.927 ± 0.027	0.929 ± 0.020
15	0.916 ± 0.025	0.863 ± 0.018
20	0.956 ± 0.027	0.951 ± 0.020

Table 4
Shielding effectiveness relative to polyethylene at discrete depths of **water** based on absorbed dose and dose equivalent.

Depth (g/cm^2)	S_D	S_H
5	0.984 ± 0.032	0.961 ± 0.023
10	0.946 ± 0.027	0.919 ± 0.020
15	0.965 ± 0.028	0.960 ± 0.021
20	0.995 ± 0.024	0.999 ± 0.018

to PE. By contrast, water is most effective at 20 g/cm^2 (proposed storm shelter thickness), even approximating the performance of polyethylene to within standard error. Moreover, as shown by Fig. 6A, water is more effective at the storm shelter depth than at the bulkhead, where the input radiation field is relatively unaltered. Looking at Fig. 6B, water is quantitatively more effective at both 15 and 20 g/cm^2 than at 5 g/cm^2. Whether based on absorbed dose (A) or dose equivalent (B), water is the only material tested here that exhibits this phenomenon. In summary, the data presented in Fig. 6 suggests that water is an effective space radiation shielding material when both target and projectile fragmentation are taken into account, while aluminum and copper are not as efficient in reducing absorbed dose and dose equivalent as a function of depth.

The error bars shown in Fig. 6 are the result of a three step process. First, the error associated with the absorbed dose measurements from the proton exposures is treated as Gaussian (or normal) since each measurement is expected to be the result of many independent processes. Second, the error associated with the absorbed dose measurements from the heavy ion exposures is computed by treating the LET fluence spectra (which are histograms) as Poisson distributions. As such, the error of a given LET interval within the spectrum is proportional to the square root of the number of occurrences. To obtain the total error of the whole spectrum, it is necessary to sum these errors on a interval-by-interval basis by first weighing each individual error with its corresponding LET interval, and then squaring the term. The error of an absorbed dose measurement taken from an LET fluence spectrum is then proportional to the square root of these integrated Poisson errors. Finally, the errors originating from the previous steps are propagated through Equation (4) using the Gaussian law of error propagation (Taylor, 1996).

5. Discussion

The approach presented here differs from previous efforts in that the measured dosimetric data is not limited to 1 GeV/n^{56}Fe exposures (La Tessa et al., 2005; Miller et al., 1998; Zeitlin et al., 2008) or computer modeling (Wilson et al., 1993). This approach possesses a number of advantages: The ability of the method to empirically account for the composition of a candidate material; carefully chosen shielding material depths relevant to the design and development of future spacecraft or planetary surface habitats; the use of a tissue-equivalent radiation detector (CR-39 PNTD). Moreover, each ion was monitored separately in order to better understand how the material modifies the primary beam as a function of shielding depth.

The two most important depths in this study were 5 g/cm^2 (bulkhead) and 20 g/cm^2 (storm shelter). In particular, the primary radiation field is relatively unaltered at bulkhead depths (5 g/cm^2) and all four materials studied here provide about the same amount of radiation protection to within standard error. However, at the storm shelter depth (20 g/cm^2) where the input radiation field has undergone significant changes, Fig. 6A and B show that water is approximately as effective as polyethylene to within standard error, while graphite, aluminum, and copper perform poorly. The favorable shielding properties observed for

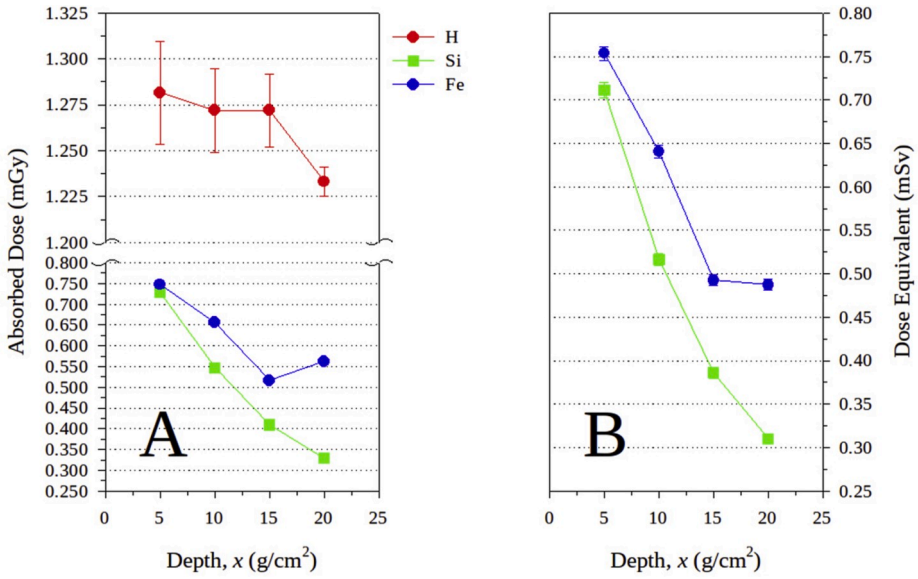

Fig. 5. The complete set of measured reference data, normalized to the front (0 g/cm^2) detector, for polyethylene; corresponding sets for aluminum, copper, graphite, and water appear qualitatively similar.

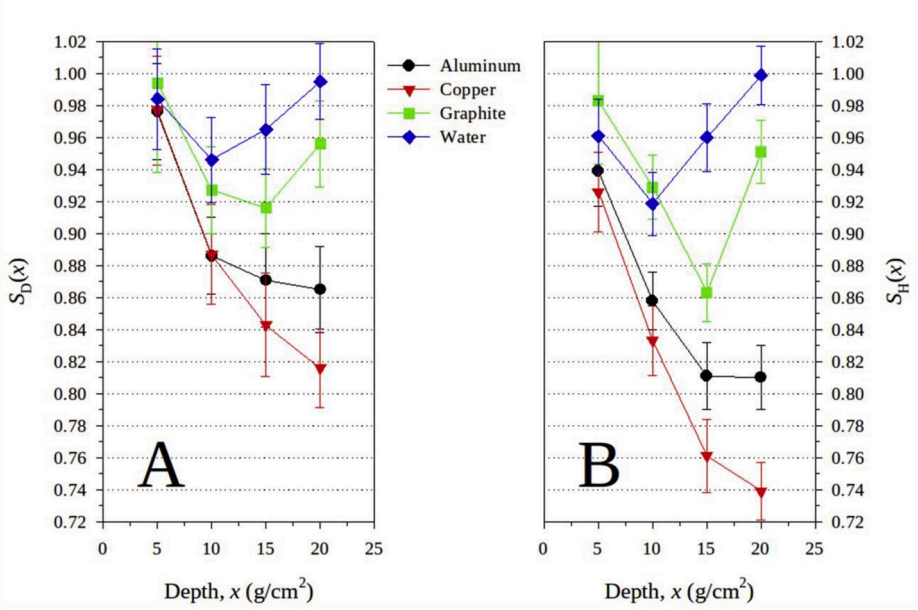

Fig. 6. Shielding effectiveness relative to polyethylene as a function of depth based on absorbed dose (A) and dose equivalent (B) for the common materials of aluminum, copper, graphite, and water.

water (see Table 4, 20 g/cm^2) could be of practical significance since water is a necessary consumable and, as such, large quantities will be required by space crews on extended interplanetary missions.

When comparing the average relative changes in shielding effectiveness based on absorbed dose, the data given in Fig. 6A provides percent fractions of approximately −5.8%, −3.9%, −1.2%, and 0.4% for copper, aluminum, graphite, and water, respectively, in descending order. This seems to indicate that water, with the lowest Z, is somewhat constant across the full range of depths studied here. This may also point to a relative balance between the increasing quantity of secondary protons produced in the shielding mass and the decreasing amount of radiation damage by heavy ions, which are relatively few. For materials such as water and polyethylene, this observation could be explained by the competing effects of target and projectile fragmentation as the radiation field evolves as a function of depth through the shielding mass. In particular, the increase in absorbed dose and dose equivalent due to an enhanced proton flux from target fragmentation could be offset by a decrease in radiation damage due to the hydrogen-induced fragmentation of heavy ion projectiles. We hypothesize a similar observation for other hydrogen-rich, low Z radiation shielding materials.

These results demonstrate an important principle of effective space radiation shielding: Namely, that low Z, high H materials are most effective at reducing absorbed dose and dose equivalent as a function of depth, while high Z materials should be avoided. This confirmation seems to indicate that the shielding effectiveness, as defined in this work by Equation (4), is formulated in a manner that is compatible with similar studies.

6. Conclusions

The goal of the present work was to develop a method to empirically quantify the space radiation shielding performance of materials applicable to the design and development of future spacecraft and planetary surface habitats. A weighted empirical quantity, the shielding effectiveness S, was developed that quantifies the efficacy of a candidate space radiation shielding material relative to polyethylene. This method used established radiation dosimetry techniques that employed Al_2O_3:C OSLDs and CR-39 PNTDs to measure the dosimetric quantities of absorbed dose and dose equivalent. The results were then weighted according to the measured percent fraction of baryonic components of the GCR spectrum, and the measured contributions (also in terms of percent fraction) to absorbed dose and dose equivalent. Each shielding effectiveness value is a synthesis of many space radiation shielding measurements made using a number of experimentally available proton and heavy ion beams. Our proposed metric supersedes that of previous efforts (Guetersloh et al., 2006; Bahadori et al., 2017) by

1. empirically accounting for the composition of a candidate material, which is especially important in the case of novel and/or complex materials;
2. carefully choosing shielding material depths relevant to the design and development of future spacecraft or planetary surface habitats;
3. using a tissue-equivalent radiation detector (CR-39 PNTD);
4. and monitoring each ion separately in order to better understand how the material modifies the primary beam as a function of shielding depth.

Additionally, this method can be used to supplement and/or verify similar findings obtained from transport models.

Whether based on absorbed dose or dose equivalent, the results in this study demonstrate the principle of effective space radiation shielding by showing that low Z materials are generally most adequate at reducing absorbed dose and dose equivalent while high Z materials tend to make the resulting radiation field more hazardous. Furthermore, this study also showed that the shielding effectiveness is generally low when based on biologically-weighted absorbed dose (dose equivalent) for a given material at a specific depth. Also of practical significance is the finding that at the bulkhead depth of 5 g/cm^2 (Fig. 6A) all materials tested in this study provide about the same amount of radiation protection to within standard error. This is not surprising since at this relatively shallow depth the input radiation field remains relatively unaltered as compared to the field at significantly greater depths.

One of the strengths of our approach is the ability of the shielding metric to display the effect of a mixed heavy ion radiation field on shielding performance in a piecewise fashion. For example, using the current data set and re-computing the shielding effectiveness of aluminum with the Fe contribution only, we can see the metric increases on average by about 3.4% across the depth range of interest. This change

in the perceived shielding performance of aluminum seems to indicate that a mixed heavy ion radiation field is important to investigate. The method presented here can accommodate an arbitrary number of beams of Z and E such that a representative sample of the GCR spectrum will enable the shielding effectiveness of a given candidate material to converge.

The data presented in Fig. 6 could give one the impression that no shielding presents less of a radiation hazard in comparison to the depths explored in this study. This observation is partially correct. On the one hand, the energetic protons of the GCR spectrum will undergo inelastic target fragmentation reactions with heavy nuclei contained in the walls of a spacecraft or planetary surface habitat. This results in a substantial increase in the flux of secondary protons in the shielding mass as a function of depth. Absorbed dose is therefore enhanced by the proton component of the GCR spectrum. By contrast, the heavy ions of the GCR spectrum will undergo projectile fragmentation with target nuclei contained in the walls of a spacecraft or planetary surface habitat. This results in the break-up of these heavy ions into fragments of reduced Z. Since absorbed dose is proportional to Z^2, this consequently leads to a reduction in the corresponding absorbed dose and dose equivalent as a function of depth. These competing processes of target versus projectile fragmentation are appropriately weighted with the coefficients a and b, respectively, in Equation (4).

The test case presented here made use of a limited set of proton and heavy ion beams to evaluate the shielding efficacy of common materials. However, the methodology outlined in this study can as well incorporate shielding data from additional beams when facilities can provide them. While the radiation shielding assessment provided here is limited to only four materials, it can serve as a foundation for future work that could improve the comprehensiveness of the shielding effectiveness approach. Implicit in the use of the shielding effectiveness—as defined by Equation (4)—is the understanding that as the number of heavy ion beams increases, so does the ability of the shielding effectiveness value to accurately represent a given material's ability to adequately shield space crews from the effects of a harmful space radiation environment.

Future work involving detailed modeling calculations could assess the minimum beam characteristics (number, type, and energy) required by this method to arrive at reliable shielding effectiveness values. On this front, it should be noted that the current study's use of direct measurements can be important when evaluating shielding candidates where the interaction cross sections used in transport models are less well known. An empirical approach could help resolve shielding performance discrepancies since many transport codes implement nuclear models that draw from the same cross section databases, possibly leading to persistent questions of whether the noted differences are accurate or simply model artifacts.

We hope that the shielding effectiveness approach described here will prove useful to spacecraft and planetary surface habitat designers and engineers in seeking alternative materials suitable for long-term space exploration missions.

Declaration of competing interest

The authors declare that they have no known competing financial interests or personal relationships that could have appeared to influence the work reported in this paper.

CRediT authorship contribution statement

J.M. DeWitt: Methodology, Software, Validation, Formal analysis, Investigation, Data curation, Writing - original draft, Writing - review & editing, Visualization. **E.R. Benton:** Conceptualization, Resources, Supervision, Project administration, Funding acquisition.

Acknowledgments

This work was supported in part by NASA MSFC Grants NAG8-01899 and NAG8-01944. The authors would like to acknowledge the generosity of NASA and the BNL in providing beam time, and the staff of the NSRL for providing support in performing irradiations. The authors also greatly appreciate the helpful discussions with Regina DeWitt and Zi-Wei Lin at East Carolina University as well as Cary Zeitlin at the Leidos Innovations Corporation.

References

Adams, J., Adcock, L., Apple, J., Christl, M., Cleveand, W., Cox, M., Dietz, K., Ferguson, C., Fountain, W., Ghita, B., 2007. Deep space test bed for radiation studies. Nucl. Instrum. Methods Phys. Res. Sect. A Accel. Spectrom. Detect. Assoc. Equip. 579, 522–525.

Armstrong, T.W., Colborn, B.L., 2001. Predictions of secondary neutrons and their importance to radiation effects inside the international space station. Radiat. Meas. 33, 229–234.

Badavi, F.F., Adams, D.O., Wilson, J.W., 2010. On the validity of the aluminum equivalent approximation in space radiation shielding applications. Adv. Space Res. 46, 719–727.

Badhwar, G.D., 1997. The radiation environment in low-earth orbit. Radiat. Res. 148, S3–S10.

Bahadori, A., Semones, E., Ewert, M., Broyan, J., Walker, S., 2017. Measuring space radiation shielding effectiveness. EPJ Web Conf. 153, 04001.

Benton, E.R., Benton, E.V., 2001. Space radiation dosimetry in low-Earth orbit and beyond. Nucl. Instrum. Methods B 184, 255–294.

Benton, E.R., Benton, E.V., Frank, A.L., 2010. Conversion between different forms of LET. Radiat. Meas. 45, 957–959.

Böhlen, T.T., Cerutti, F., Chin, M.P.W., Fassò, A., Ferrari, A., Ortega, P.G., Mairani, A., Sala, P.R., Smirnov, G., Vlachoudis, V., 2014. The FLUKA code: developments and challenges for high energy and medical applications. Nucl. Data Sheets 120, 211–214.

Brown, K., Ahrens, L., Hung Chiang, I., Gardner, C., Gassner, D., Hammons, L., Harvey, M., Kling, N., Morris, J., Pile, P., 2010. The NASA space radiation laboratory at Brookhaven National Laboratory: preparation and delivery of ion beams for space radiation research. Nucl. Instrum. Methods Phys. Res. 618, 97–107.

Cartwright, B.G., Shirk, E.K., Price, P.B., 1978. A nuclear-track-recording polymer of unique sensitivity and resolution. Nucl. Instrum. Methods 153, 457–460.

Cassou, R.M., Benton, E.V., 1978. Properties and applications of CR-39 polymeric nuclear track detector. Nucl. Track Detect. 2, 173–179.

Cucinotta, F.A., Durante, M., 2006. Cancer risk from exposure to galactic cosmic rays: implications for space exploration by human beings. Lancet Oncol. 7, 431–435.

Cucinotta, F.A., Kim, M.-H.Y., Chappell, L.J., 2012. Evaluating Shielding Approaches to Reduce Space Radiation Cancer Risks, NASA TM-2012-217361. NASA Johnson Space Center.

Cucinotta, F.A., 2014. Space radiation risks for astronauts on multiple international space station missions. PloS One 9 (4), e96099. https://doi.org/10.1371/journal.pone.0096099.

Cucinotta, F.A., Cacao, E., 2017. Non-targeted effects models predict significantly higher Mars mission cancer risk than targeted effects models. Nat. Sci. Rep. 7, 1832.

DeWitt, J.M., Benton, E.R., Uchihori, Y., Yasuda, N., Benton, E.V., Frank, A.L., 2009. Assessment of radiation shielding materials for protection of space crews using CR-39 plastic nuclear track detector. Radiat. Meas. 44, 905–908.

Dreute, J., Trakowski, W., Schöfer, B., Brechtmann, C., Drechsel, H., Eversberg, H., Fricke, W., Beer, J., Wiegel, B., Heinrich, W., 1986. The siegen automatic measuring system for nuclear track detectors: status and new developments. Nucl. Tracks 12, 261–264.

Durante, M., Cucinotta, F.A., 2011. Physical basis of radiation protection in space travel. Rev. Mod. Phys. 83, 1245–1281.

Durante, M., 2014. Space radiation protection: destination Mars. Life Sci. Space Res. 1, 2–9.

Ferrari, A., Sala, P.R., Fassò, A., Ranft, J., 2005. FLUKA: a Multi-Particle Transport Code. CERN-2005-10, INFN/TC_05/11, SLAC-R-773.

Guetersloh, S., Zeitlin, C., Heilbronn, L., Miller, J., Komiyama, T., Fukumura, A., Iwata, Y., Murakami, T., Bhattacharya, M., 2006. Polyethylene as a radiation shielding standard in simulated cosmic-ray environments. Nucl. Instrum. Methods Phys. Res. Sect. B Beam Interact. Mater. Atoms 252, 319–332.

Henke, R.P., Ogura, K., Benton, E.V., 1986. Standard method for measurement of bulk etch in CR-39. Nucl. Tracks 12, 307–310.

Konradi, A., Cucinotta, F.A., 1997. Shielding Strategies for Human Space Exploration, NASA CP-3360. NASA Langley Research Center.

La Tessa, C., Guetersloh, S., Heilbronn, L., Miller, J., Sihver, L., Zeitlin, C., 2005. Fragmentation of 1 GeV/nucleon iron ions in thick targets relevant for space exploration. Adv. Space Res. 35, 223–229.

McKeever, S.W.S., 2011. Optically stimulated luminescence: a brief overview. Radiat. Meas. 46, 1336–1341.

Miller, J., Zeitlin, C., Heilbronn, L., Borak, T., Carters, T., Frankel, K.A., Fukumurad, A., Murakami, T., Rademacher, S.E., Schimmerling, W., Stronach, C., 1998. Ground-based simulations of cosmic-ray heavy ion interactions in spacecraft and planetary habitat shielding materials. Acta Astronaut. 42, 389–394.

Noll, A., Rusch, G., Rocher, H., Dreute, J., Heinrich, W., 1988. The siegen automatic measuring system for nuclear track detectors: new developments. Nucl. Tracks Radiat. Meas. 15, 265–368.
Norbury, J.W., Schimmerling, W., Slaba, T.C., Azzam, E.I., Badavi, F.F., Baiocco, G., Benton, E., Bindi, V., Blakely, E.A., Blattnig, S.R., Boothman, D.A., Borak, T.B., Britten, R.A., Curtis, S., Dingfelder, M., Durante, M., Dynan, W.S., Eisch, A.J., Zeitlin, C.J., 2016. Galactic cosmic ray simulation at the NASA space radiation laboratory. Life Sci. Space Res. 8, 38–51.
National Research Council, 2008. Managing Space Radiation Risk in the New Era of Space Exploration. National Academy Press, Washington, DC.
Riley, P., 2012. On the probability of occurrence of extreme space weather events. Space Weather 10, S02012.
Rink, W., Thompson, J. (Eds.), 2013. Earth Sciences Series. Encyclopedia of Scientific Dating Methods: SpringerReference. Springer-Verlag Berlin Heidelberg. https://doi.org/10.1007/SpringerReference_359042.
Rusch, G., Winkel, E., Noll, A., Heinrich, W., 1991. The siegen automatic measuring system for track detectors: new developments. Nucl. Tracks Radiat. Meas. 19, 261–266.
Sawakuchi, G.O., Yukihara, E.G., McKeever, S.W.S., Benton, E.R., Gaza, R., Uchihori, Y., Yasuda, N., Kitamura, H., 2008. Relative optically stimulated luminescence and thermoluminescence efficiencies of Al_2O_3:C dosimeters to heavy charged particles with energies relevant to space and radiotherapy dosimetry. J. Appl. Phys. 104, 124903.
Shavers, M.R., Zapp, N., Barber, R.E., Wilson, J.W., Qualls, G., Toupes, L., Ramsey, S., Vinci, V., Smith, G., Cucinotta, F.A., 2004. Implementation of ALARA radiation protection on the ISS through polyethylene shielding augmentation of the Service Module Crew Quarters. Adv. Space Res. 34, 1333–1337.
Sihver, L., 2008. Physics and biophysics experiments needed for improved risk assessment in space. Acta Astronaut. 63, 886–898.
Simonsen, L.C., Wilson, J.W., Kim, M.-H.Y., Cucinotta, F.A., 2000. Radiation exposure for human Mars exploration. Health Phys. 79, 515–525.
Simpson, J.A., 1983. Elemental and isotropic composition of the galactic cosmic rays. Annu. Rev. Nucl. Part Sci. 33, 323–381.
Slaba, T.C., Wilson, J.W., Badavi, F.F., Reddell, B.D., Bahadori, A.A., 2015. Solar Proton Transport within an ICRU Sphere Surrounded by a Complex Shield: Ray-Trace Geometry. NASA TP 2015-218994.
Taylor, J.R., 1996. An Introduction to Error Analysis: the Study of Uncertainties in Physical Measurements, second ed. University Science Books, Sausalito, CA.
Thibeault, S.A., Kim, M.-H.Y., Wilson, J.W., Long, E.R.J., Kiefer, R.L., Glasgow, M.B., Orwoll, R.A., 1997. Shielding materials development and testing issues. In: Shielding Strategies for Human Space Exploration, NASA CP-3360. NASA Langley Research Center.
Townsend, L.W., Wilson, J.W., Shinn, J.L., Curtis, S.B., 1992. Human exposure to large solar particle events in space. Adv. Space Res. 12, 339–348.
Trakowski, W., Schöfer, B., Dreute, J., Sonntag, S., Brechtmann, C., Beer, J., Drechsel, H., Heinrich, W., 1984. An automatic measuring system for particle tracks in plastic detectors. Nucl. Instrum. Methods Phys. Res. 225, 92–100.
Weaver, B.A., Westphal, A.J., 2002. Energy loss of relativistic heavy ions in matter. Nucl. Instrum. Methods Phys. Res. Sect. B Beam Interact. Mater. Atoms 187, 285–301.
Wiegel, B., Beer, J., Fricke, W., Eversberg, H., Heinrich, W., 1986. Cosmic ray LET-spectra investigated by automatic scanning and measuring of plastic nuclear track detectors. Nucl. Tracks 12, 515–518.
Wilson, J.W., Wood, J.S., Shinn, J.L., Cucinotta, F.A., Nealy, J.E., 1993. A Proposed Performance Index for Galactic Cosmic Ray Shielding Materials, NASA TM-4444. NASA Langley Research Center.
Wilson, J.W., Badavi, F.F., Cucinotta, F.A., Shinn, J.L., Badhwar, G.D., Silberberg, R., Tsao, C.H., Townsend, L.W., Tripathi, R.K., 1995. HZETRN: Description of a Free-Space Ion and Nucleon Transport and Shielding Computer Program, NASA TP-3495. NASA Langley Research Center.
Wilson, J.W., Shinn, J.L., Simonsen, L.C., Cucinotta, F.A., Dubey, R.R., Jordan, W.R., Jones, T.D., Chang, C.K., Kim, M.-H.Y., 1997. Exposures to Solar Particle Events in Deep Space Missions, NASA TP-3668. NASA Langley Research Center.
Wilson, J.W., Cucinotta, F.A., Shinn, J.L., Simonsen, L.C., Dubey, R.R., Jordan, W.R., Jones, T.D., Chang, C.K., Kim, M.-H.Y., 1999. Shielding from solar particle event exposures in deep space. Radiat. Meas. 30, 361–382.
Wilson, J.W., Cucinotta, F.A., Kim, M.-H.Y., Schimmerling, W., 2001a. Optimized shielding for space radiation protection. Phys. Med. 17, 67–71.
Wilson, J.W., Shinn, J.L., Tripathi, R.K., Singleterry, R.C., Clowdsley, M.S., Thibeault, S.A., Cheatwood, F.M., 2001b. Issues in deep space radiation protection. Acta Astronaut. 49, 289–312.
Wilson, J.W., Slaba, T.C., Badavi, F.F., Reddell, B.D., Bahadori, A.A., 2015. Solar Proton Transport within an ICRU Sphere Surrounded by a Complex Shield: Combinatorial Geometry, NASA TP 2015-218980.
Zeitlin, C., Guetersloh, S., Heilbronn, L., Miller, J., Elkhayari, N., Empl, A., LeBourgeois, M., Mayes, B.W., Pinsky, L., Christl, M., Kuznetsov, E., 2008. Shielding experiments with high-energy heavy ions for spaceflight applications. New J. Phys. 10, 075007.
Zeitlin, C., Hassler, D.M., Cucinotta, F.A., et al., 2013. Measurements of energetic particle radiation in transit to Mars on the Mars science laboratory. Science 340, 1080–1084.
Zeitlin, 2016. Personal communication.
Zhou, D., 2012. CR-39 Plastic Nuclear Track Detectors in Physics Research. Nova Science Publishers, New York.